Coulomb explosion induced by intense ultrashort laser pulses in two-dimensional clusters

Vincent Mijoule,[1,2,*] Laurent J. Lewis,[2,†] and Michel Meunier[1,‡]
[1]*Département de Génie Physique et Regroupement Québécois sur les Matériaux de Pointe (RQMP), École Polytechnique de Montréal, Case Postale 6079, Succursale Centre-Ville, Montréal, Québec, Canada H3C 3A7*
[2]*Département de Physique et Regroupement Québécois sur les Matériaux de Pointe (RQMP), Université de Montréal, Case Postale 6128, Succursale Centre-Ville, Montréal, Québec, Canada H3C 3J7*
(Received 11 October 2005; published 23 March 2006)

The phenomenon of Coulomb explosion is studied through qualitative numerical simulations of clusters irradiated with intense ultrashort laser pulses. We introduce a semiquantum approach which allows us to model two different types of materials—akin to rare gases and dielectrics—and which is appropriate for both low- and high-energy domains, i.e., the thermodynamic regime and the Coulomb explosion regime. Through a detailed study of clusters submitted to laser pulses of various intensities, we demonstrate that Coulomb explosion is the process responsible for cluster explosion under femtosecond laser pulses. We examine the differences in the dynamics of explosion of rare-gas clusters as a function of the wavelength of the incident laser radiation. For dielectric clusters, our simulations reveal a fragmented explosion mechanism; the influence of the size of the cluster is also studied.

DOI: 10.1103/PhysRevA.73.033203 PACS number(s): 36.40.Qv, 78.20.Bh, 36.40.Gk, 31.15.Qg

I. INTRODUCTION

During the last decade, the concept of Coulomb explosion has emerged as a fundamental phenomenon underlying the dynamics of condensed matter irradiated by very intense and very short laser pulses. Since the introduction of the theoretical foundations [1], extensive work has been carried out, both experimentally [2–4] and theoretically [5], to understand the mechanisms leading to Coulomb explosion.

The recent advent of femtosecond lasers has made it possible to ionize matter extremely quickly, i.e., on time scales for which the nuclei stay fixed; the resulting positive space charge has been assumed to play an important role in various physical processes, such as rare-gas cluster explosion, laser ablation, and nanoparticle fragmentation. It has been demonstrated [2,3] that the ions emitted by the explosion of rare-gas clusters present a strong degree of correlation between charge and energy, suggesting that the mechanism is of electrostatic origin and invalidating previous analysis based on hydrodynamic models. A similar charge-energy correlation has been reported in the case of ions expelled from surfaces by laser ablation [6]. Last, Coulomb repulsion has been assumed to play a key role in the nonthermal fragmentation of metallic nanoparticles [7].

Most theoretical investigations of Coulomb explosion have dealt with rare-gas clusters exposed to infrared laser pulses. Recent papers, corroborating experimental results, have focused on an exhaustive description of the explosion dynamics, including electron heating processes [8,9], plasma [8,10], and ionization [11–14] mechanisms, and nuclei acceleration [15–17]. However, most of these studies have been carried out within the framework of classical models, using particle-in-cell [18,19] or molecular dynamics computer simulation codes. These approaches have brought several important insights into the physics of the problem. Yet, considering the electrons as point particles poses the problem of the electronic screening of the nuclei repulsion, and thus of the stability of the low-energy states. The recent works of Rusek *et al.* [20] and Fennel *et al.* [21] must be mentioned as first attempts to solve this problem by using a Thomas-Fermi electron-gas model and a Thomas-Fermi-Vlasov method, respectively.

In the present work, we introduce a simple, yet powerful, semiquantum model based on the Madelung hydrodynamic formulation of quantum mechanics, which turns out to present some similarities with the model of Rusek *et al.* In essence, the model consists in representing the electron density of probability "fluid," $\int|\psi(\vec{r},\vec{r}_2,\ldots,\vec{r}_n)|^2 d\vec{r}_2\cdots d\vec{r}_n$, where $\psi(\vec{r}_1,\vec{r}_2,\ldots,\vec{r}_n)$ is the wave function of the n-electron system, by an ensemble of pseudoparticles, thus establishing the parallel with macroscopic fluids. Our model intrinsically takes into account the quantum nature of matter, thus allowing a proper description of the behavior of the systems at both low energies (thermodynamical regime) and high energies (Coulomb explosion regime).

We use this approach to study two-dimensional models for rare-gas-like clusters (containing 73 atoms) irradiated by sub- and above-band-gap laser pulses (i.e., long- and short-wavelength pulses relative to the material absorption threshold), as well as dielectriclike clusters (73 and 685 atoms) under sub-band-gap laser pulses, in both cases at various intensities; the meaning of "rare-gas" and "dielectric" in the present context is explained below. Our method provides a complete description of rare-gas clusters under sub-band-gap pulses, i.e., in the multiphoton absorption regime, and thus confirms the predominance of Coulomb explosion in the explosion dynamics in this case. For above-band-gap pulses, our results extend those of Rusek *et al.*, and reveal a crossover from hydrodynamic expansion to Coulomb explosion in

*Electronic address: vincent.mijoule@m4x.org
†Electronic address: Laurent.Lewis@UMontreal.CA
‡Electronic address: michel.meunier@polymtl.ca

the cluster dynamics. Last, we study dielectric clusters and the influence of size on the explosion mechanism, and demonstrate that Coulomb explosion is the dominant mechanism in this case too; our results reproduce the observed nonthermal fragmentation of nanoparticles. We begin with a brief description of the model.

II. METHODOLOGY

A. Quantum fluid dynamics equations

As noted earlier, most studies of Coulomb explosion have been carried out using essentially classical models. Since the very first simulations of clusters [22], several improvements have been proposed to take into account the fundamentally quantum character of matter (i.e., tunnel effect, molecular binding, etc.). As an example, one can mention the Ammosov-Delone-Krainov equations [23] for the tunnel ionization of electrons. However, in all of these approaches, the electrons are treated as point particles, thus making it impossible to explicitly take into account the molecular binding between the atoms. In fact, the inherent instability of charged-particle systems forbids any regime other than Coulomb explosion to be studied, i.e., the Coulomb explosion is, in some sense, built into the models. As explained in detail below, the present model resolves this problem by regarding the electrons as delocalized particles, in contrast to the point-particle approach of the usual classical models. It is based on the Madelung formulation of the Schrödinger equation, also called quantum fluid dynamics (QFD). (See Ghosh *et al.* [24] for an exhaustive review.) Our model thus allows the simultaneous study of both thermal and Coulomb explosion regimes which, as we will demonstrate, is a definite advantage.

The Madelung equations are obtained by a transformation of the Schrödinger equation into a continuity equation and an Euler-type equation of motion. Writing the time-dependent wave function $\psi(\vec{r}_1,\vec{r}_2,\ldots,\vec{r}_n,t)$ of an n-electron system subject to a potential $V(\vec{r}_1,\vec{r}_2,\ldots,\vec{r}_n,t)$—basically the potential of the ions plus the electronic repulsions—as

$$\psi(\vec{r}_1,\vec{r}_2,\ldots,\vec{r}_n,t) = R(\vec{r}_1,\vec{r}_2,\ldots,\vec{r}_n,t)e^{iS(\vec{r}_1,\vec{r}_2,\ldots,\vec{r}_n,t)/\hbar}, \quad (1)$$

the time evolution of R and S is given by

$$\frac{\partial\rho}{\partial t} + \vec{\nabla}\cdot(\rho\vec{v}) = 0 \quad (2a)$$

and

$$m_e\rho\left(\frac{\partial\vec{v}}{\partial t} + (\vec{v}\cdot\vec{\nabla})\vec{v}\right) = -\rho\vec{\nabla}(V + V_{qu}), \quad (2b)$$

where m_e is the mass of the electron, with

$$\rho = R^2, \quad (3a)$$

$$\vec{v} = \vec{\nabla}S/m_e, \quad (3b)$$

$$V_{qu} = -\frac{\hbar^2}{2m_e}\frac{\vec{\nabla}^2 R}{R}. \quad (3c)$$

One can immediately see the similarity of the time evolution equations for the electron density probability fluid with those for a classical macroscopic fluid. The main difference lies in the additional purely quantum potential V_{qu}. Because they are expressed in terms of two real numbers—the density of the fluid ρ and its velocity $\vec{v}$—the QFD formulation of quantum mechanics is more intuitive than the Schrödinger formulation, expressed in terms of a complex probability amplitude.

In order to exploit the QFD equations, it is necessary to project them from the multi-dimensional space onto real space, since ρ and $\vec{v}$ are functions of the n position variables $\vec{r}_1,\vec{r}_2,\ldots,\vec{r}_n$. To this effect, we introduce the two projected quantities

$$\rho_0(\vec{r},t) = \int \rho(\vec{r},\vec{r}_2,\ldots,\vec{r}_n,t)d\vec{r}_2\cdots d\vec{r}_n \quad (4)$$

and

$$\vec{v}_0(\vec{r},t) = \frac{\int \rho(\vec{r},\vec{r}_2,\ldots,\vec{r}_n,t)\vec{v}_1(\vec{r},\vec{r}_2,\ldots,\vec{r}_n,t)d\vec{r}_2\cdots d\vec{r}_n}{\int \rho(\vec{r},\vec{r}_2,\ldots,\vec{r}_n,t)d\vec{r}_2\cdots d\vec{r}_n}. \quad (5)$$

Note that $\vec{v}=(\vec{v}_1,\vec{v}_2,\ldots,\vec{v}_n)$ in Eq. (3b). Upon integrating Eqs. (2a) and (2b) over the $n-1$ variables $\vec{r}_2,\ldots,\vec{r}_n$, we obtain the equations of motion for ρ_0 and $\vec{v}_0$ assuming the existence of a certain functional $\vec{F}$:

$$\frac{\partial\rho_0}{\partial t} + \vec{\nabla}\cdot(\rho_0\vec{v}_0) = 0 \quad (6a)$$

and

$$m_e\rho_0\left(\frac{\partial\vec{v}_0}{\partial t} + (\vec{v}_0\cdot\vec{\nabla})\vec{v}_0\right) = \vec{F}(\rho_0,\vec{v}_0) - \rho_0\vec{\nabla}(V_0). \quad (6b)$$

The functional $\vec{F}$ describes the motion of the electron fluid in absence of the "external" potential V_0 (the potential of the ions). It is certainly a very complicated object which cannot be computed in practice; it includes the electronic Coulomb repulsion and the quantum potential V_{qu}. To a first approximation, it is responsible for the spreading of the electron wave functions. The laser interaction will be taken in account by simply adding the electric force $-\rho ne\vec{E}$ in the right-hand side of Eq. (6b).

As a central feature of our model, by analogy with macroscopic fluids, we represent the probability fluid ρ_0 by an ensemble of pseudoparticles. The density of probability fluid of the n-electron system is represented by nN point pseudoparticles (N per electron), whose mass and charge are m_e/N and $-e/N$, respectively; the electrons are thus delocalized in the present model. From Eq. (6b), one sees that the pseudoparticles are subject to external forces, as in the case of (classical) point electrons. More specifically, the action of F is introduced via a repulsive force between the pseudoparticles; this force is chosen empirically and consequently can be adjusted according to the type of material considered

(here, rare gas or dielectric), as discussed in detail in the following section. As usual, the nuclei are also considered as classical point particles, a reasonable approximation in view of their large mass compared to that of the electron. Finally, we assume that each atom possesses a single electron, which is sufficient for the purpose of the present qualitative study of Coulomb explosion.

The advantage of this approach is that both the ions and the electron pseudoparticles can be dealt with using the standard molecular-dynamics toolbox. One need only define the three types of interactions involved: ion-ion, ion-pseudoparticle, and pseudoparticle-pseudoparticle. The first two are simply Coulombic. However, in order to avoid the singularity of the Coulomb force, the force is taken proportional to $(r/(r+\alpha)^3)$, where $\alpha=0.1$ Å; note that both interactions are treated in the same manner in order to ensure the "universality" of the Coulomb potential and avoid unphysical effects. The interaction between pseudoparticles is chosen empirically, depending on the type of material under consideration, with, however, the following constraints: it must be Coulombic at long range—since we are dealing with electrons—and stronger than Coulomb at short distances in order to prevent the electron pseudoparticles from collapsing on the nuclei. The potentials used in the present study are described below.

Other computational details are as follows. The number of pseudoparticles per electron N is chosen equal to 10; while not large, this value is sufficient to ensure proper physical behaviour while allowing relatively large systems to be dealt with. The equations of motion were integrated using the Verlet algorithm with a time step of 10^{-18} s. A 1 ps run takes about 2 h for a 73-atom cluster (803 particles in total) on a good personal computer.

B. Interaction potentials

The pseudoparticle-pseudoparticle interaction can be adjusted so as to describe different types of materials. In the present case, it was chosen to represent two different materials: the first has properties similar to those of rare gases; and the second would be typical of a generic solid insulator which we will simply call "dielectric." This must of course be understood very loosely, as our model is meant to be qualitative rather than quantitative. The following conditions were imposed in determining the potentials: First, the electron cloud should have the "correct" size (1–2 Å) and possess an acceptable distribution around the nuclei; this will be illustrated below. Second, the interatomic potential should be Lennard-Jones-like (attractive at long range and repulsive at short range), with an equilibrium distance of a few (3–4) angstroms, and a binding energy of a few hundred Kelvin for rare-gas atoms or a few thousand Kelvin for dielectrics. Last, the absorption spectrum should be typical of the material studied. The expression of the potentials are given explicitly in the Appendix.

The search for the potentials $V_{e\text{-}e}$ is otherwise intuitive and empirical. In practice, the potential is first tested on a simple one-atom system (i.e., the hydrogen atom). It is verified that the electron pseudoparticles are correctly localized around the nucleus. A two-atom system is examined next. The initial state of the system is as follows. The two nuclei are fixed at a given distance and the electron pseudoparticles are relaxed so that the electrons can reach their ground state. (The system is not globally in its ground state since the nuclei are not at the minimum-energy distance.) The nuclei are then given a small velocity toward one another and released; they first attract, then repel, and the energy is calculated as a function of distance. Finally, the potentials are tested on clusters; the ground state is obtained in two steps: first, relaxation of the pseudoparticles with fixed nuclei, then relaxation of the whole system.

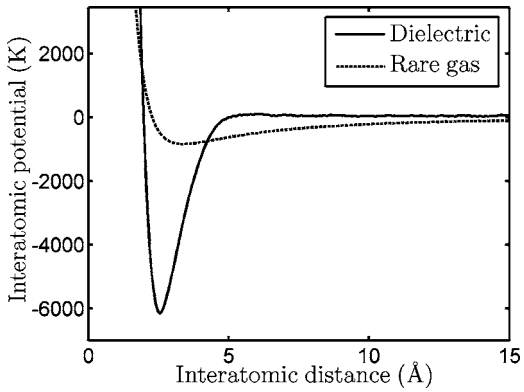

FIG. 1. Interatomic potentials as a function of distance, for rare-gas atoms (dotted line) and dielectric atoms (full line).

The interatomic potentials for the two materials considered here are displayed in Fig. 1. One observes that the potentials are very much Lennard-Jones shaped, with equilibrium distances and binding energies typical of rare gases and dielectrics, respectively. The corresponding 73-atom clusters are presented in Fig. 2; as expected, the systems possess the usual triangular structure (modulo the distortions induced by the surfaces). One important difference between the two clusters is already visible: the electron clouds in the rare-gas cluster are (as they should be) much more localized in the immediate vicinity of the nuclei than in the dielectric cluster, suggesting an electronic binding between the nuclei. The present method thus yields ground-state configurations which are realistic. In addition, the configurations were found to be long lived, the clusters exhibiting a realistic thermodynamic behaviour over extended periods of time.

We have performed light absorption simulations on the 73-atom clusters in order to confirm the nature of the materials. To do this, we calculated the energy absorbed by the clusters for very low intensities and long laser pulses at various frequencies. The results are presented in Fig. 3. The two clusters exhibit a threshold in energy below which light is not absorbed—as expected much larger in the rare-gas cluster than in the dielectric cluster.

III. RARE-GAS CLUSTERS IRRADIATED BY SUB-BAND-GAP PHOTONS

A. Results and observations

We have performed a series of calculations at various laser intensities (i.e., various values of the electric field) for the

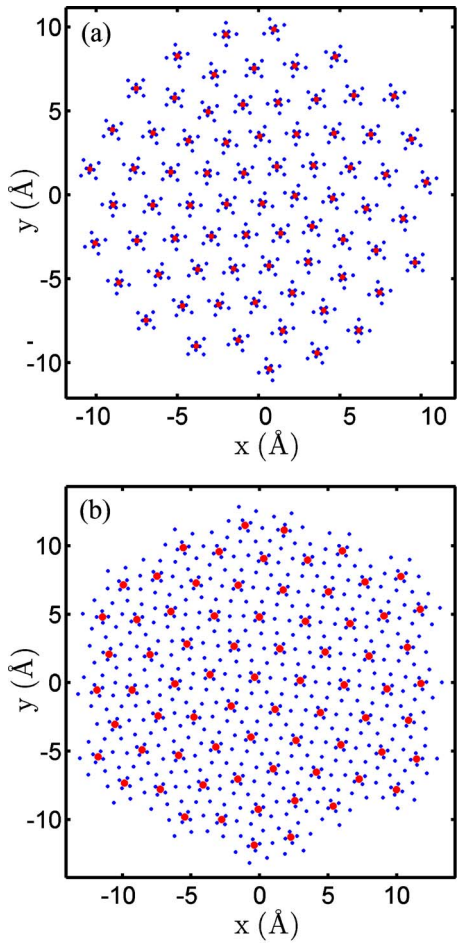

FIG. 2. (Color online) Top view of (a) the 73-atom rare-gas cluster and (b) the 73-atom dielectric cluster in their ground states. The large dots represent the nuclei and the small dots represent the electron pseudoparticles. Note that some electron pseudoparticles are not clearly seen in the figure because they are too close to the nuclei.

rare-gas cluster. The cluster, initially given a temperature of a few Kelvin, is illuminated with a 100 fs pulse, Gaussian in time, arriving "from the top" (z direction). The laser frequency ω is set to 1.59×10^{14} Hz, corresponding to a long-wavelength photon with energy much lower than the gap. The laser is circularly polarized; this choice is arbitrary but will be useful for undertanding the results of the simulations, as it is consistent with the symmetry of the clusters. The associated electric field varies from 0 to 4.3×10^{10} V m^{-1}. As an indication, the latter value of the electric field would correspond in the three-dimensional case to an intensity of 5.6×10^{13} W cm^{-2}. The results of the simulations after 1 ps are presented in Fig. 4 in terms of energy of the nuclei, electronic energy, ionization level (i.e., fraction of the electrons ejected), and external radius of the cluster.

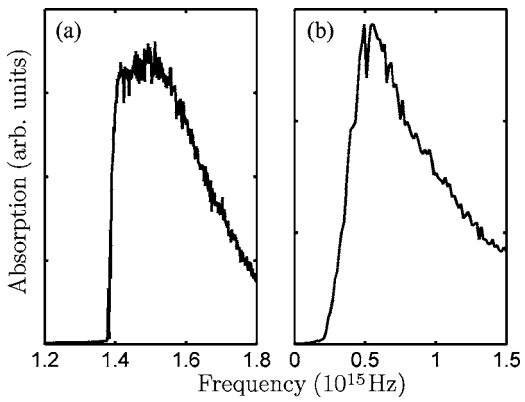

FIG. 3. Absorption spectrum for (a) the 73-atom rare-gas cluster and (b) the 73-atom dielectric cluster.

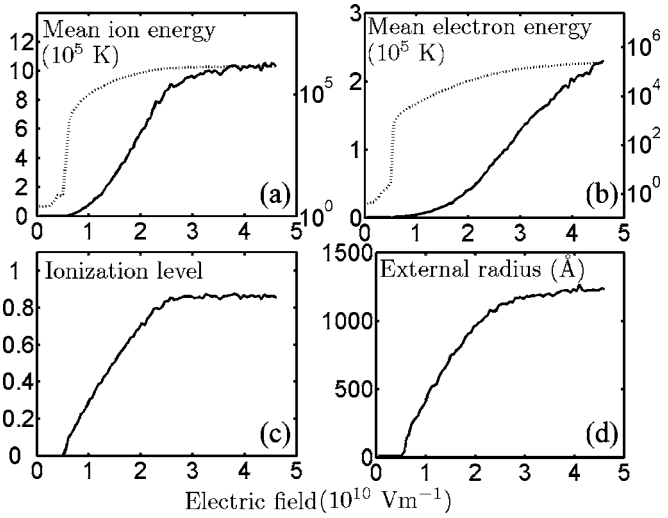

FIG. 4. Characteristics of the 73-atom rare-gas cluster irradiated by a long-wavelength pulse, after 1 ps, as a function of electric field (i.e., laser intensity): (a) mean ion energy (dashed line, logarithmic scale); (b) mean electron energy, obtained by summing the pseudoparticle energies (dashed line, logarithmic scale); (c) ionization level, i.e., fraction of the electrons that have been ejected out of the cluster; (d) external radius, defined as the distance from the most distant ion to the center of the initial cluster.

Our simulations reveal, and this is a most notable feature, a sudden change in the behavior of the cluster at a value of the electric field **E** of about 0.5×10^{10} V m^{-1}. A slight variation of **E** dramatically changes the response of the system in the "critical" zone: as can be seen clearly in Fig. 4(a), the mean ion energy increases by many orders of magnitude at the critical intensity; the ionization process begins [Fig. 4(c)] and the cluster starts expanding [Fig. 4(d)]. The transition between the two regimes is perhaps best appreciated from the electronic energy, shown in Fig. 4(b). The critical intensity is the ablation threshold.

Below the critical intensity, the energy transferred from the laser to the solid is very low, almost unobservable. Indeed, the electrons are just weakly excited, with no influence on the nuclei dynamics, and evidently no ionization. The cluster is "transparent." Above the critical intensity, the laser light gives rise to a sufficient density of photons in the cluster to induce multiphoton absorption. (Recall that the photon energy is much lower than the gap.) This strongly nonlinear state can be divided into two stages, as we now discuss.

(1) The first stage occurs at relatively low intensities, just above the ablation threshold. The kinetic energy of the nuclei

and the ionization level of the cluster increase dramatically as the laser intensity increases; the cluster eventually explodes, more violently so at larger intensities, as can be appreciated from the external radius of the cluster, which increases with the intensity. During the laser pulse (100 fs), part of the electrons are ejected from the cluster; the remaining electrons are no longer coherent with the (still) well-organized ground-state structure. Electron pseudoparticles hop from one ion to another, indicating that the system is in an excited state. However, the great mobility of the free electrons is such that they reorganize very quickly about the ions (within a few femtoseconds); as a result, there is no obvious local (atomic-scale) irregularity in the electron density once the pulse has passed. A few tens of femtoseconds after the beginning of the pulse, the nuclei have acquired a significant amount of energy and the cluster explodes. The fundamental mechanism underlying such an increase in ion energy over such a short period of time (1 ps) is obviously nonthermal. We will demonstrate in the following section that this phenomenon is the Coulomb explosion.

(2) At higher intensities, for $\mathbf{E} \gtrsim 3 \times 10^{10}$ V m^{-1}, the intensity of the explosion saturates. Indeed, beyond a given laser intensity, almost all the electrons have been ejected so that further increasing the intensity does not change the behavior of the system.

In order to study the critical zone between nonablation and ablation regimes in more detail, additional simulations have been performed using pulse durations of 25, 50, and 200 fs. In fact, because of the strongly nonlinear sensitivity of the system to the applied field, the pulse duration is an appropriate parameter for tuning the energy transmitted to the cluster and for studying the critical regime.

The critical intensity (or ablation threshold) is essentially independent of the pulse duration because it depends on the photon energy and on the energy gap. However, the critical zone, i.e., the zone over which a partial explosion takes place (see below), does depend on the pulse duration, and spreads over an increasing range of intensities as the pulse duration decreases. This is clearly demonstrated in Fig. 5, where the ion energy distribution as a function of intensity for different pulse durations is displayed.

In the critical zone, the explosion is partial: the external layers of the cluster are ejected but the core remains more or less bound, then evolves thermally. The transition between the two regimes discussed above is continuous, and results in the splitting (indicated by the black diagonal line) of the distribution in terms of high-energy ions (outer shells) and low-energy ions (core). As the intensity increases, the population of high-energy ions increases and that of low-energy ions decreases, until the explosion is total. These observations will be further discussed in the following sections.

B. Coulomb explosion

In order to ensure that the ejection process is indeed due to a Coulomb explosion, and not the consequence of a hydrodynamic process, we plot in Fig. 6 the relation between the mean ion energy $\bar{E}$ and the mean ion charge $\bar{Q}$, both taken at the end of the simulation (i.e., after 1 ps). Ishikawa

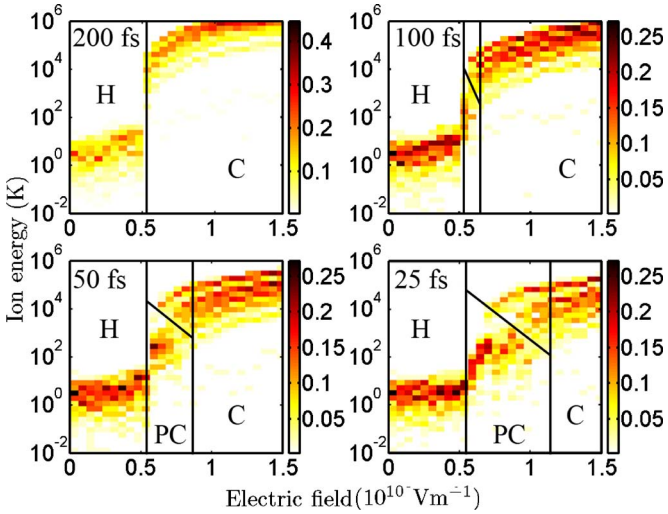

FIG. 5. (Color online) Ion energy distribution after 1 ps for different pulse durations (200, 100, 50, 25 fs). The critical regime is outlined by the two vertical lines. The diagonal line separates high- and low-energy atoms, thus marking the Coulomb explosion; H=hydrodynamics; C=Coulomb explosion; PC=partial Coulomb explosion.

et al. [16] have proposed a method to distinguish the Coulomb explosion regime from the hydrodynamic expansion regime which we briefly summarize here.

In a Coulomb explosion, the electrostatic potential energy of the charged ions is converted into kinetic energy. Since the potential energy has a quadratic dependence on the charge of the ions, the mean ion energy $\bar{E}$ should be proportional to the square of the mean charge $\bar{Q}$. The data of Fig. 6 indicate that this is indeed the case, within statistical uncertainty, for high ionization levels. In the hydrodynamic regime, now, the energy transferred to the ions is the thermal energy of the hot electrons, which is proportional to $\frac{3}{2}k_b\bar{Q}T_e$ (k_b is the Boltzmann constant) [1]. Assuming that the electronic temperature T_e does not depend much on $\bar{Q}$, the hydrodynamic regime should exhibit a linear energy-charge relation. However, $\bar{Q}$ and T_e both depend on the laser intensity; T_e therefore depends on $\bar{Q}$ implicitly and the energy-charge relation may

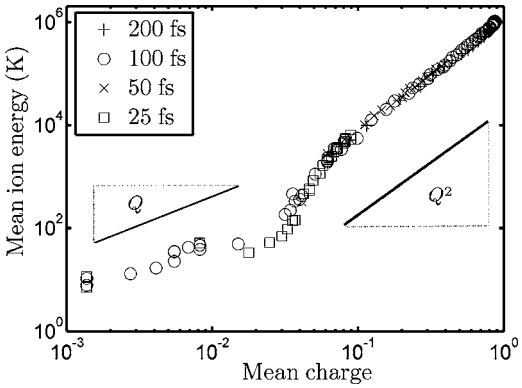

FIG. 6. Mean energy of the ions as a function of the mean charge, for different pulse durations. The laser intensity is an implicit parameter.

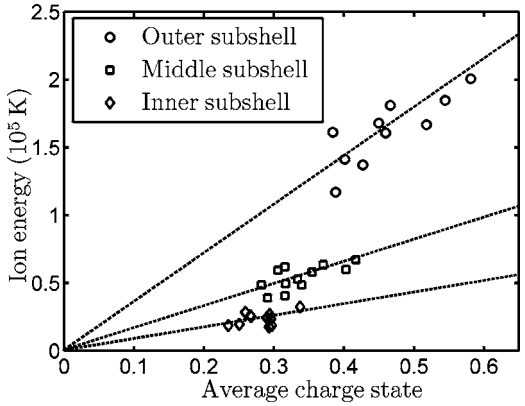

FIG. 7. Energy of the ions as a function of charge state, for ions belonging to three different portions of the cluster (inner, middle, and outer subshell), at the end of the simulation, for an electric field of 0.8×10^{10} V m^{-1} and a pulse duration of 100 fs.

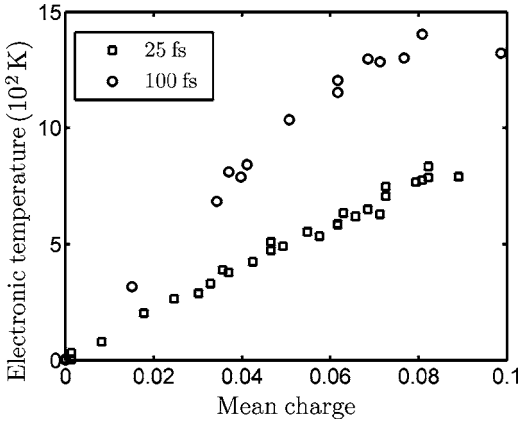

FIG. 8. Electronic temperature as a function of mean charge for 100 and 25 fs pulses.

not be that simple. Nevertheless, it appears to be roughly linear, as indicated in Fig. 6. In any case, a crossover from the high-energy Coulomb explosion regime to a low-energy regime is clearly visible at $\bar{Q}\approx0.05-0.1$; the latter, as will be demonstrated below, is the hydrodynamic regime.

Only the Coulomb explosion regime leads to significant ion energies, and therefore this is obviously the mechanism responsible for the disintegration of the cluster. This can be further established by examining the correlation between the ion energies and the charges for three different categories of atoms: inner, middle, and outer subshells; this is done in Fig. 7. We find a roughly linear relationship for each group. The origin of this relationship is not clear, but the fact that the ions with a larger charge are more energetic is the unambiguous signature of an electrostatic process, i.e., Coulomb explosion.

C. Hydrodynamic expansion

The low-energy regime, which corresponds to low ionization levels, is governed by the electronic temperature. Indeed, for a given mean charge, we observe that the energy of a cluster exposed to a 100 fs laser pulse is higher than that of a cluster exposed to a 25 fs laser pulse. Now, at the same time, the electronic temperature is also higher for longer pulses, as demonstrated in Fig. 8. This correlation clearly indicates that the low-energy regime, which is dominated by electronic excitations, is the hydrodynamic regime, as mentioned above. In this regime, clusters expand as a result of the electronic pressure, which itself increases with electronic temperature.

Thus, as shown in Fig. 8, electron heating is more efficient with a long pulse at smaller intensity than with a shorter pulse at higher intensity and, as a consequence, a shorter pulse has to be more intense to yield the same number of ejected electrons. This can be explained as follows. Electron heating is caused by inverse bremsstrahlung, i.e., the collisions of the electron gas with the electrostatic field of the ions. The collisions occur at two levels: microscopic, where the electrons are scattered by individual ions [15], and macroscopic, where they are collectively scattered by all of the ions [14]. Thus, it is the duration of the pulse which determines the electron heating rather than the laser intensity: the number of oscillations of the electron gas is more relevant than the amplitude of these oscillations.

Figure 8 shows that the ionization process does not depend on the electronic temperature: different values of T_e can indeed lead to the same ionization level using, e.g., different pulse durations. The process which leads to the ejection of electrons is field ionization, not electron heating. Indeed, the flux of outgoing electrons is directly linked to the intensity of the laser, as demonstrated in Fig. 9.

These processes—electronic heating and field ionization—are different in the case of above-band-gap pulses, and will be reexamined in Sec. IV. Our results are fully consistent with previous studies [9,15], which drew the same conclusions about the ionization processes.

D. Partial Coulomb explosion

The splitting of the ion energy distribution observed in Fig. 5 is, as already discussed, a consequence of the partial Coulomb explosion, and is directly related to the nonuniform distribution of electrons in the cluster. Indeed, we observe the electron density to be higher in the core than in the outer

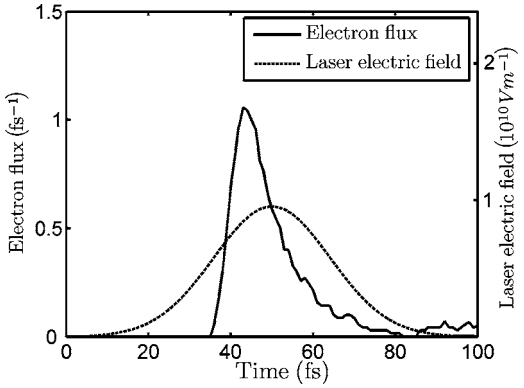

FIG. 9. Flux of ejected electrons as a function of time for a 100 fs pulse and an electric field of 0.91×10^{10} V m^{-1}.

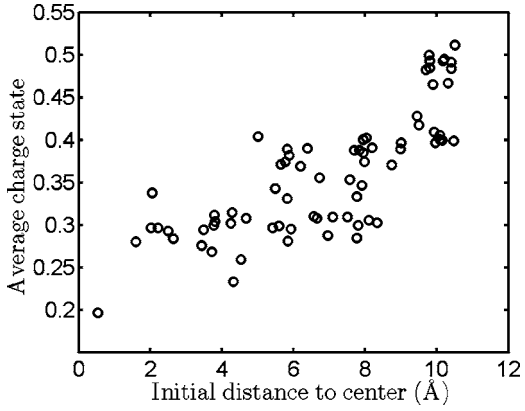

FIG. 10. Charge of the atoms versus initial distance to the center of the cluster at the end of the simulation (1 ps), for a laser electric field $\mathbf{E}=0.91\times10^{10}$ V m^{-1} and a pulse duration of 100 fs. The charges are averaged over time.

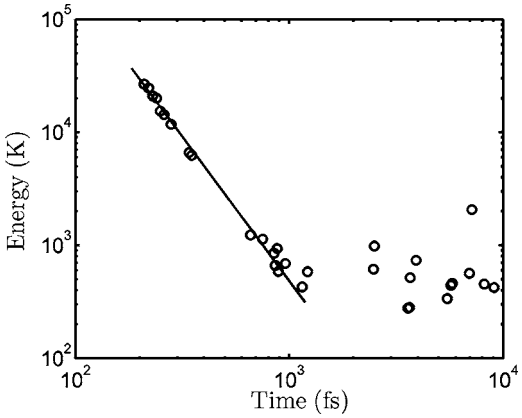

FIG. 11. Energy versus time of ejection of the ions, for a pulse duration of 25 fs and a laser electric field of 0.8×10^{10} V m^{-1}.

shells. This observation does not agree with the results of Rusek *et al.* [15], although it is rather intuitive: Consider the electrostatic potential induced by the nuclei; the latter is higher in the core region. Thus, even if the electrons in the core may detach more easily from their nuclei, as discussed in Ref. [11], the electron density will tend to be larger than in the outer shells, and the ions will be less ionized. This is verified in Fig. 10, where we plot the charge of the atoms as a function of their initial distance from the center of the cluster, after 1 ps and for $\mathbf{E}=0.91\times10^{10}$ V m^{-1}.

The positive space charge, therefore, increases toward the outer layers of the cluster. The outer ions thus feel a significant electric field and, at the same time, they possess a large positive charge. In contrast, the atoms located near the center of the cluster are weakly charged and are subject to a weak electric field. For a certain degree of ionization, the electron screening can thus be sufficient to cancel the repulsive force in the core of the cluster but not in the outer shells. As a result, the inner atoms may remain bound, leading to a partial dissociation of the cluster. As the intensity of the pulse increases, more electrons are ejected and the remaining cluster becomes smaller and smaller, until the explosion is total.

In the previous section, we have shown that, at constant ionization level, a longer pulse yields a higher electronic temperature than a shorter pulse. The clusters, which only partially explode for short pulses, therefore totally decompose for long pulses: the high temperature of the electron gas causes the ions to heat and, eventually, the cluster to dissociate totally via hydrodynamic expansion, although the energy this process delivers is negligible compared to that released through Coulomb explosion. For short pulses, a partial explosion occurs because a great quantity of electrons is ejected, such that the electron screening no longer can ensure the global cohesion of the solid; at the same time, the electrons are not heated much, preventing that part of the cluster which has not been ejected to undergo hydrodynamic expansion.

It is interesting to study the evolution of partially exploded clusters for longer times; to this end, we have performed additional simulations over 10 ps. After the expansion of the inner shells, due to the increase of the electronic temperature, the energy is converted into heat through electron-ion and ion-ion interactions. The temperature of the cluster increases continuously, and some atoms are vaporized. We can then distinguish three phases for the partial Coulomb explosion: A first phase, of the order of 100 fs, where electrons are ejected; a second phase, of the order of 100–1000 fs, where high-energy, charged ions are ejected due to Coulomb explosion; and a third phase, much longer, where low-energy atoms are vaporized. The two last phases are illustrated in Fig. 11, where each point represents an atom crossing an imaginary circle of radius $r_0=30$ Å around the cluster. We can easily distinguish two groups of points. A first group which crosses the circle in the first 1000 fs: these correspond to the Coulomb-ejected atoms, i.e., the first outer shells; the observed relation $E\sim t^{-2}$ simply reflects the fact that more energetic ions (higher velocities) arrive at the circle before less energetic ones (i.e., $E\sim v^2$ and $v=r_0/t$). The second group of points correspond to the core atoms which thermally vaporize starting about 3 ps after the beginning of the simulation, at random times and with random energies. These results agree with experimental observations of laser ablation [25].

IV. RARE-GAS CLUSTERS IRRADIATED BY ABOVE-BAND-GAP PHOTONS

We turn now to a corresponding study of the irradiation of rare-gas clusters by above-band-gap (short-wavelength) pulses. Here $\omega=1.59\times10^{15}$ Hz, a tenfold increase compared to the long-wavelength case. This frequency is above the absorption threshold and the material is therefore no longer transparent. The energy absorbed by the cluster varies continuously; it does not vanish at small intensities and there is no critical intensity. Likewise, the electronic temperature varies continuously. Two series of simulations were carried out, for pulse durations of 25 and 100 fs, respectively; in both cases the laser intensity (electric field) was varied. The results for the 100 fs pulse are presented in Fig. 12.

The ionization process here is different than for sub-band-gap pulses: the direction of the electric field of the laser now changes very quickly, and no field ionization is possible. The

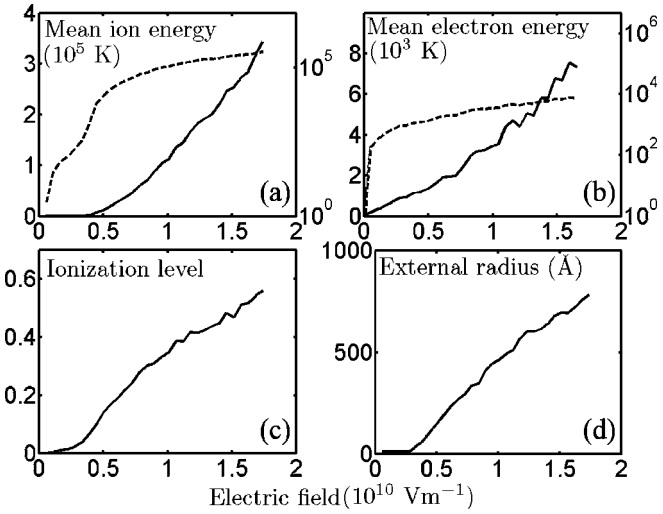

FIG. 12. Characteristics of the 73-atom rare-gas cluster irradiated by a short-wavelength pulse, after 1 ps, as a function of electric field (i.e., laser intensity): (a) mean ion energy (dashed line, logarithmic scale); (b) mean electron energy, obtained by summing the pseudoparticle energies (dashed line, logarithmic scale); (c) ionization level, i.e., fraction of the electrons that have been ejected out of the cluster; (d) external radius, defined as the distance from the most distant ion to the center of the initial cluster.

ionization of the cluster is actually a consequence of electron-electron collisions. Indeed, these processes thermalize the electrons, which gain energy by colliding with the nuclei; some of the highest-energy electrons can then escape the cluster. We plot in Fig. 13 the flux of outgoing electrons together with the electronic temperature. After the end of the pulse, the flux decreases, since the number of electrons remaining in the cluster is less, and the electronic temperature decreases.

The mechanism of explosion also differs from the long-wavelength case. For a given level of ionization, the electronic temperature is higher for above-band-gap pulses than for sub-band-gap pulses, as shown in Fig. 14, in particular at small values of the charge. This result is a consequence of the ionization process prevailing in both situations: electron-electron collisions for short-wavelength pulses (which correlates with the electronic temperature) and field ionization for long-wavelength pulses.

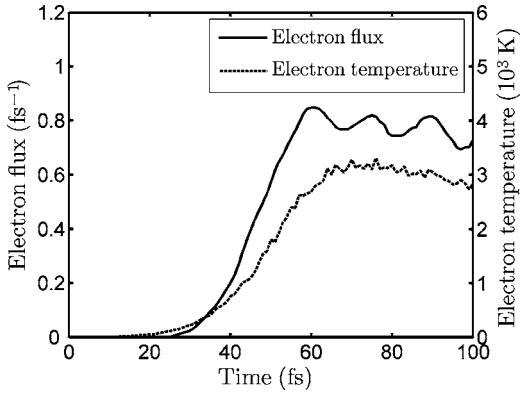

FIG. 13. Flux of ejected electron and electronic temperature as a function of time, for a 100 fs pulse and an electric field of 5.1×10^9 V m^{-1}.

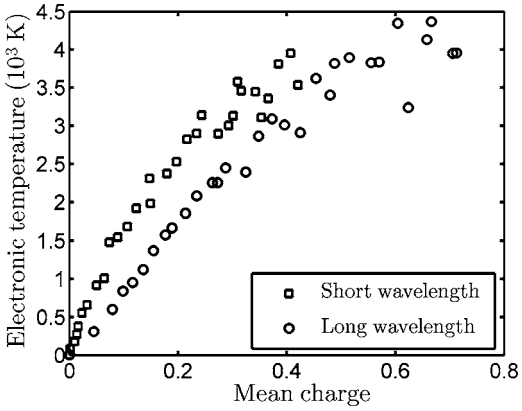

FIG. 14. Comparison of the electronic temperature as a function of the mean charge for sub-band-gap (long-wavelength) pulses and above-band-gap (short-wavelength) pulses.

As a result of the higher electron temperature, the hydrodynamic regime is more dominant for above-band-gap photons. This can in fact be verified in Fig. 12(a): two regimes in energy can be distinguished, $\mathbf{E}<0.25\times10^{10}$ V m^{-1} and $\mathbf{E}>0.25\times10^{10}$ V m^{-1}; these correspond to the hydrodynamic and the Coulomb regime, respectively, whereas only Coulomb was observable in the case of sub-band-gap irradiation—compare Figs. 12(a) and 4(a). In the latter case, because the photons have lower energy, the electron temperature never reaches a point where the hydrodynamic regime may become important: the dynamics is exclusively dominated by the Coulomb explosion regime.

The crossover between the two regimes is thus smoother in the case of short-wavelength pulses, as can be observed in Fig. 15. For low ionization levels ($\bar{Q}\lesssim0.05$), the hydrodynamic regime is stronger for above-band-gap pulses, reducing the possibility of a partial explosion. This effect is also visible in the distribution of ion energies: we observe that the splitting between high and low energies is smaller than in the long-wavelength case, and the width of the critical zone is

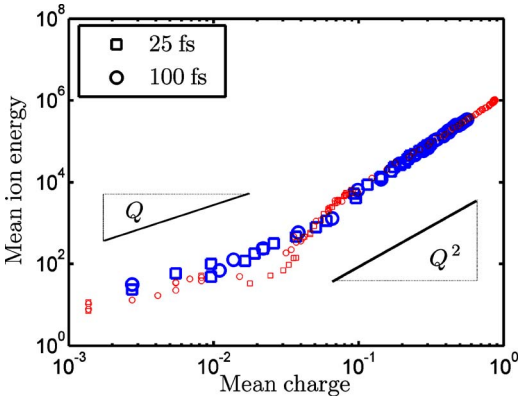

FIG. 15. (Color online) Mean ion energy versus mean charge for rare-gas clusters irradiated by 25 and 100 fs laser pulses, at the end of the simulation, i.e., after 1 ps. Large (blue) symbols, above-band-gap irradiation; small (red) symbols, sub-band-gap irradiation.

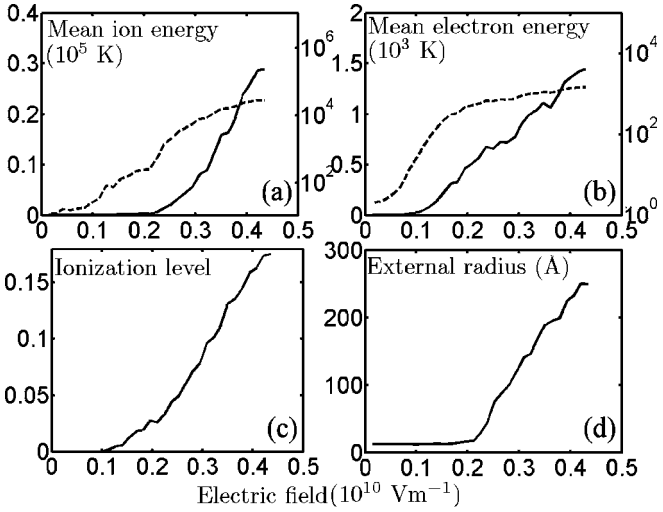

FIG. 16. Characteristics of the 73-atom dielectric cluster irradiated by a long-wavelength pulse, after 1 ps, as a function of electric field (i.e., laser intensity): (a) mean ion energy (dashed line, logarithmic scale); (b) mean electron energy, obtained by summing the pseudoparticle energies (dashed line, logarithmic scale); (c) ionization level, i.e., fraction of the electrons that have been ejected out of the cluster; (d) external radius, defined as the distance from the most distant ion to the center of the initial cluster.

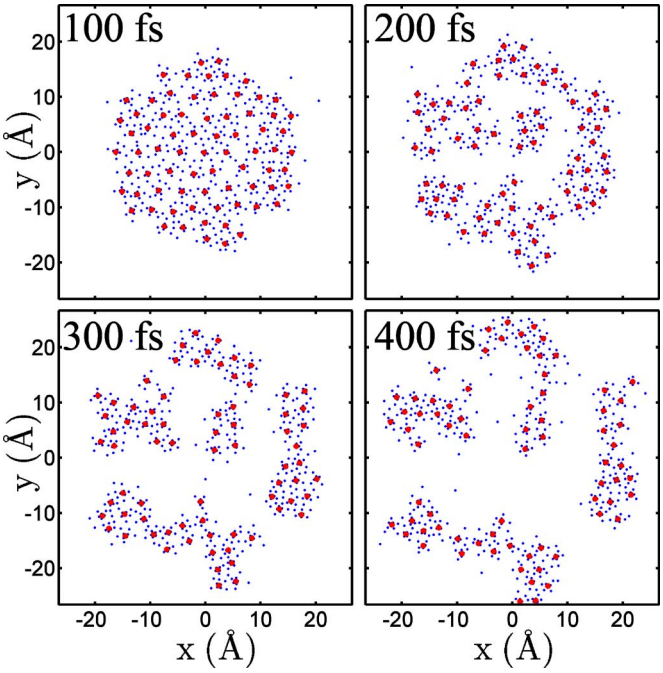

FIG. 17. (Color online) View of the 73-atom dielectric cluster at various times, as indicated, for a 100 fs pulse, with $\mathbf{E}=0.24\times10^{10}$ V m^{-1}.

also smaller. For high ionization levels ($\bar{Q}\gtrsim0.05$), in contrast, the Coulomb explosion regime is slightly weaker for short-wavelength irradiations. This can be understood as follows: previous to the Coulomb explosion, the hydrodynamic expansion increases the distances between the ions, reducing the positive electrostatic potential energy and leading to lower final energies for the ions. Otherwise, the Coulomb explosion regime for short-wavelength pulses is similar to that for long-wavelength pulses; indeed, the linear relation between mean ion energy and ion charge for each subshell is still observed.

V. DIELECTRIC CLUSTERS IRRADIATED BY SUB-BAND-GAP PHOTONS

The study of dielectric clusters follows along the same lines as that for rare-gas clusters. Again here, simulations have been carried out for 25 and 100 fs laser pulses, as well as two cluster sizes (73 and 685 atoms). In both cases, the laser is circularly polarized, has a Gaussian shape in time and a frequency of 1.59×10^{14} Hz, well below the threshold for absorption, and corresponding to the long-wavelength case for the rare-gas clusters. The results for the 100 fs simulations of the 73-atom cluster as a function of laser intensity are presented in Fig. 16.

Since the gap is here much smaller than in the rare-gas case, we expect the threshold field for nonlinear effects to be lower. Below 0.05×10^{10} V m^{-1}, indeed, the laser irradiation is not absorbed by the electrons. Above this value, the electrons start to be excited and two regimes can be distinguished. First, between 0.05×10^{10} and 0.2×10^{10} V m^{-1}, the hydrodynamic behavior dominates, as can be judged from the ion energy after 1 ps. This regime is characterized by a slow increase of the energy with laser intensity. Second, above 0.2×10^{10} V m^{-1}, the ion energy increases rapidly; this corresponds to the Coulomb explosion regime. We return to a detailed discussion of these two regimes below.

The results are similar for a 25 fs pulse, and no partial Coulomb explosion is observed. The energy distribution exhibits no splitting at all. The absence of a partial Coulomb explosion regime can be understood by the visual inspection of the cluster at various times, as shown in Fig. 17. In a dielectric material, the atoms are much more tightly bound than in a rare gas. As a consequence, surface atoms do not easily detach during the Coulomb explosion. Rather, the system "releases the pressure" by a fragmentation process similar to that observed in silicon [26] and Lennard-Jones solids [27,28] the positive space charge left behind the outgoing electrons causes the cluster to enter a metastable state, since the cohesion of the cluster can no longer be ensured with such a low number of electrons and such a state of excitation. The clusters fragment; the Coulomb potential energy is converted into surface energy and kinetic energy (of the fragments). No splitting is observed in the energy distribution because the atoms in a given fragment all have roughly the same kinetic energy. This phenomenon may be related to the non-thermal fragmentation of nanoparticles observed by Link *et al.* [7].

The fragmentation process can be monitored in terms of the surface energy, which is proportional to the surface of the cluster; this is displayed in Fig. 18. The higher the laser intensity (and thus the ionization level), the higher the surface energy, and thus the larger the number of small clusters. Figure 18 shows that the surface energy saturates at very high intensities; this is because the Coulomb explosion is

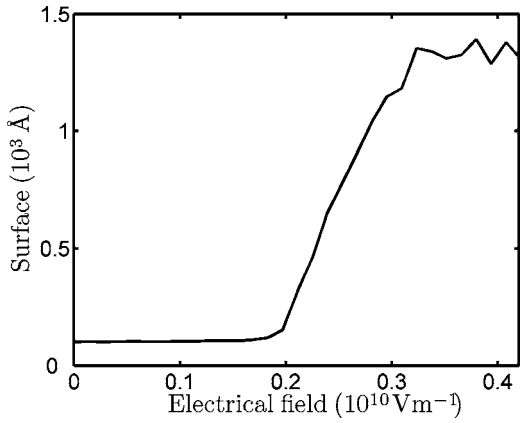

FIG. 18. Surface of the cluster, which is proportional to the surface energy, as a function of the electric field, at the end of the simulation.

total—the system has fragmented into individual ions.

As in the case of rare-gas clusters, we are interested in determining the range of laser intensities over which hydrodynamic expansion and Coulomb explosion operate. This can be done by examining, again, the relation between mean ion energy and mean ion charge, shown in Fig. 19. For high ionization levels, we find again a quadratic relation between mean energy and mean charge, which is the signature of the Coulomb explosion. The crossover to the hydrodynamic regime is observed around 0.04. In this regime, it appears that the mean energy is higher for a 100 fs pulse than for a 25 fs pulse, for the same ionization level. This is, once more, a consequence of the higher electron temperature observed for 100 fs pulses. We conclude, again, that the hydrodynamic regime dominates only for low ionization levels.

It can be surprising that the Coulomb explosion occurs for such low levels of ionization in the present case, where the weakness of the binding cannot be invoked as in the case of rare-gas clusters. A possible explanation is as follows. In dielectric materials, the energy gap is smaller, and the electrons can more easily be freed. For a given number of ejected

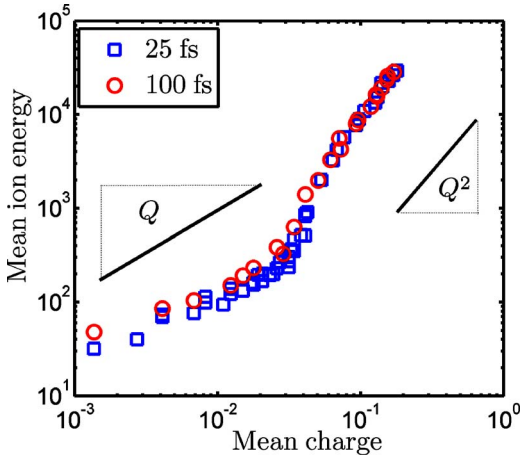

FIG. 19. (Color online) Mean ion energy as a function of the ionization level for the 73-atom dielectric clusters, at the end of the simulation.

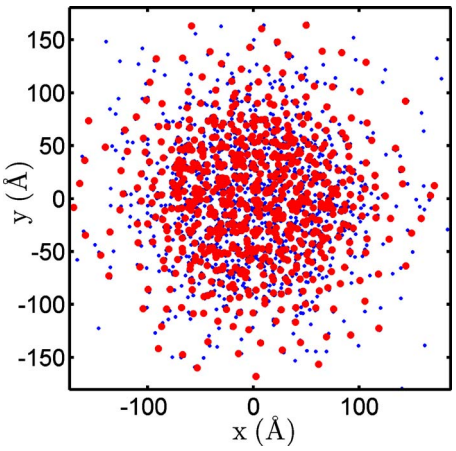

FIG. 20. (Color online) View of the 685-atom cluster after 800 fs, for an electric field of 0.39×10^{10} V m^{-1} Vm and a pulse duration of 100 fs.

electrons, the inner ionization state in the dielectric will be higher than in the rare gas, since a large number of free electrons will remain in the cluster. A few electrons thus remain bound to the ions, thereby diminishing the electronic screening and decreasing the binding forces between the ions.

Finally, corresponding simulations have been performed for a dielectric cluster containing 685 atoms. We find that the threshold electric field is roughly the same as for the 73-atom cluster. Also, the ionization level is lower, at a given laser intensity, for the 685-atom cluster. The field ionization process is the reason of this observation: During the irradiation of the cluster, the electron cloud is driven by the electric field of the laser and then oscillates with a given amplitude. This amplitude does not depend on the cluster size. However, the "overflow" of the electron gas out of the cluster is larger, relatively speaking, in the smaller cluster than in the larger cluster, and thus the ionization level is also larger.

The explosion of the 685-atom cluster occurs for ionization levels as low as 0.01. This can be explained easily using a scaling argument. Consider a uniformly charged solid sphere of radius r; the total potential repulsive energy scales as r^5. Since the number of atoms n in the sphere scales as r^3, the potential energy scales as $n^{5/3}$, or $n^{2/3}$ per atom. In the two-dimensional case, the total potential energy scales as r^3 and the number of atoms n in the charged disc as r^2, so that the potential energy scales as $\sqrt{n}$ per atom. The repulsive energy is thus larger for larger clusters, leading to a Coulomb explosion at lower ionization levels. Using a similar argument, one finds that the outer atoms are subject to a much larger Coulomb force. During the Coulomb explosion regime, the external shells are thus ejected as single ions, while the core of the cluster is fragmented, in contrast with the case of the 73-atom cluster. This is clearly visible in Fig. 20.

For the 685-atom cluster, the expansion takes much longer than for the 73-atom clusters. Plotting the mean ion energy, as we have done previously in order to determine the regime of expansion, is thus irrelevant, since the energy is not yet totally released after 800 fs, the duration of our simulations. We can however examine the relation between the

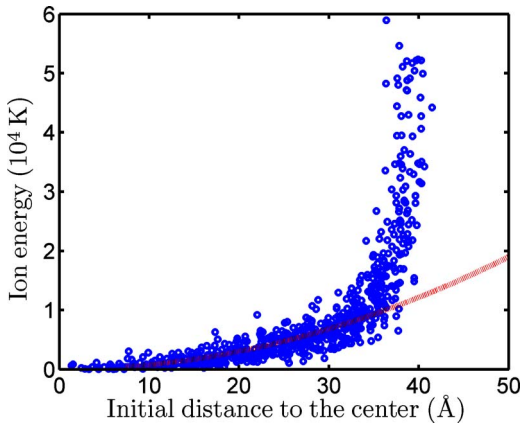

FIG. 21. (Color online) Ion energy after 800 fs versus initial distance to the center, for an electric field of 0.39×10^{10} V m^{-1}. The (red) line is a guide to the eye for low-energy ions.

final energy of each ion versus its initial distance to the center of the cluster, for an intermediate electric field; this is displayed in Fig. 21. The break in the curve confirms, as suggested earlier, that two different types of expansion are active—fragmented explosion for the inner shells of the cluster and isolated-atom Coulomb explosion for the outer shells—and seems to indicate a concomitant action of the hydrodynamic and Coulomb explosion regimes for intermediate ionizations.

VI. SUMMARY AND CONCLUDING REMARKS

We have presented a study of the Coulomb explosion of small model clusters—two dimensional, one electron per atom, "reasonable" interaction potentials—using a simple, yet powerful, semiquantum model which reproduces the essential features of the physical systems under consideration. Our results are in qualitative agreement with the results reported previously for rare-gas clusters; we demonstrated in particular that Coulomb explosion is responsible for the disintegration of the clusters. We also discussed how the dynamics of clusters is affected by the wavelength of the laser, especially ionization and electronic heating, and how the clusters behave around the threshold laser intensity. We have also presented an attempt to simulate Coulomb explosion in dielectrics; our calculations reveal additional mechanism in this case, viz., fragmentation.

Our work opens the way to further simulations in which both Coulomb explosion and hydrodynamic expansion need be taken into account. In particular, our model would be useful for simulations of laser ablation, for which a part of the irradiated surface undergoes Coulomb explosion.

ACKNOWLEDGMENTS

Useful discussions with Patrick Lorazo and Danny Perez are gratefully acknowledged. This work has been supported by grants from the Natural Sciences and Engineering Research Council of Canada (NSERC) and the Fonds Québécois de la Recherche sur la Nature et les Technologies (FQRNT). We are grateful to the Réseau Québécois de Calcul de Haute Performance (RQCHP) for generous allocations of computer resources.

APPENDIX: ELECTRON PSEUDOPARTICLE INTERACTIONS

The electron pseudoparticle interaction potentials mentioned in Sec. II B are presented below. Actually, it is more convenient to present the forces derivating from these potentials.

For the rare-gas material, the interaction force $\vec{f}_{pseudo}(\vec{r})$ is given by

$$\vec{f}^{rg}_{pseudo}(\vec{r}) = \frac{e^2}{4\pi\epsilon_0 N^2}\left(\frac{\vec{r}}{(r+0.1)^3}\frac{r}{r+0.45} + 0.358\frac{\vec{r}}{(r^2+0.01)^2}\right). \tag{A1}$$

For the dielectric material, it is given by

$$\vec{f}^{di}_{pseudo}(\vec{r}) = \begin{cases} \dfrac{e^2}{4\pi\epsilon_0 N^2}\dfrac{\vec{r}}{(r+0.1)^3} & \text{if } r \geqslant 3 \text{ Å}, \\ 1.549\dfrac{e^2}{4\pi\epsilon_0 N^2}\dfrac{\vec{r}}{(r^2+0.005)^2} & \text{if } \leqslant 3 \text{ Å}. \end{cases} \tag{A2}$$

All the distances are assumed to be expressed in angstroms.

[1] T. Ditmire, T. Donnelly, A. M. Rubenchik, R. W. Falcone, and M. D. Perry, Phys. Rev. A **53**, 3379 (1996).
[2] H. Wabnitz *et al.*, Nature (London) **420**, 482 (2002).
[3] M. Lezius, S. Dobosz, D. Normand, and M. Schmidt, Phys. Rev. Lett. **80**, 261 (1997).
[4] F. Dorchies, T. Caillaud, F. Blasco, C. Bonté, H. Jouin, S. Micheau, B. Pons, and J. Stevefelt, Phys. Rev. E **71**, 066410 (2005).
[5] V. P. Krainov and M. B. Smirnov, Phys. Rep. **370**, 237 (2002).
[6] R. Stoian, M. Boyle, A. Thoss, A. Rosenfeld, G. Jorn, I. V. Hertel, and E. E. B. Campbell, Appl. Phys. Lett. **80**, 353 (2002).
[7] S. Link, C. Burda, M. B. Mohamed, B. Nikoobakht, and M. A. El-Sayed, J. Phys. Chem. A **103**, 1165 (1999).
[8] S. V. Fomichev, D. F. Zaretsky, D. Bauer, and W. Becker, Phys. Rev. A **71**, 013201 (2005).
[9] U. Saalmann and J.-M. Rost, Phys. Rev. Lett. **91**, 223401 (2003).
[10] T. Taguchi, T. M. Antonsen, and H. M. Milchberg, Phys. Rev. Lett. **92**, 205003 (2004).
[11] V. Véniard, R. Taieb, and A. Maquet, Phys. Rev. A **65**, 013202 (2001).

[12] U. Saalmann and J.-M. Rost, Phys. Rev. Lett. **89**, 143401 (2002).
[13] I. Last and J. Jortner, Phys. Rev. A **60**, 2215 (1999).
[14] C. Jungreuthmayer, M. Geissler, J. Zanghellini, and T. Brabec, Phys. Rev. Lett. **92**, 133401 (2004).
[15] M. Rusek and A. Orlowski, Phys. Rev. A **71**, 043202 (2005).
[16] K. Ishikawa and T. Blenski, Phys. Rev. A **62**, 063204 (2000).
[17] I. Last and J. Jortner, Phys. Rev. A **62**, 013201 (2000).
[18] A. Pukhov, J. Plasma Phys. **61**, 425 (1999).
[19] M. Eloy, R. Azambuja, J. T. Mendonca, and R. Bingham, Phys. Plasmas **8**, 1084 (2001).
[20] M. Rusek, H. Lagadec, and T. Blenski, Phys. Rev. A **63**, 013203 (2001).
[21] T. Fennel, G. F. Bertsch, and K. H. Meiwes-Broer, Eur. Phys. J. D **29**, 367 (2004).
[22] C. Rose-Petruck, K. J. Schafer, K. R. Wilson, and C. P. J. Barty, Phys. Rev. A **55**, 1182 (1997).
[23] M. Ammosov, N. B. Delone, and V. P. Krainov, Sov. Phys. JETP **64**, 1191 (1986).
[24] S. K. Ghosh and B. M. Deb, Phys. Rep. **92**, 1 (1982).
[25] R. Stoian, A. Rosenfeld, D. Ashkenasi, I. V. Hertel, N. M. Bulgakova, and E. E. B. Campbell, Phys. Rev. Lett. **88**, 097603 (2002b).
[26] P. Lorazo, L. J. Lewis, and M. Meunier, Phys. Rev. Lett. **91**, 225502 (2003).
[27] D. Perez and L. J. Lewis, Phys. Rev. B **67**, 184102 (2003).
[28] D. Perez and L. J. Lewis, Phys. Rev. Lett. **89**, 255504 (2003b).